Acta Astronautica 68 (2011) 1113–1125

Contents lists available at ScienceDirect

Acta Astronautica

journal homepage: www.elsevier.com/locate/actaastro

A vectorial bootstrapping approach for integrated GNSS-based relative positioning and attitude determination of spacecraft

Peter J. Buist [a,*], Peter J.G. Teunissen [a,b], Sandra Verhagen [a], Gabriele Giorgi [a]

[a] DEOS, Delft University of Technology, Kluyverweg 1, 2629 HS, Delft, The Netherlands
[b] Department of Spatial Sciences, Curtin University of Technology, Perth, Australia

ARTICLE INFO

Article history:
Received 3 June 2010
Accepted 25 September 2010
Available online 15 October 2010

Keywords:
GNSS/GPS
Kinematic relative positioning
Multi-antenna
Hardware-in-the-loop simulation
Attitude determination

ABSTRACT

Traditionally in multi-spacecraft missions (e.g. formation flying, rendezvous) the GNSS-based relative positioning and attitude determination problem are treated as independent. In this contribution we will investigate the possibility to use multi-antenna data from each spacecraft, not only for attitude determination, but also to improve the relative positioning between spacecraft. Both for ambiguity resolution and accuracy of the baseline solution, we will show the theoretical improvement achievable as a function of the number of antennas on each platform. We concentrate on ambiguity resolution as the key to precise relative positioning and attitude determination and will show the theoretical limit of this kind of approach. We will use mission parameters of the European Proba-3 satellites in a software-based algorithm verification and a hardware-in-the-loop simulation. The software simulations indicated that this approach can improve single epoch ambiguity resolution up to 50% for relative positioning applying the typical antenna configurations for attitude determination. The hardware-in-the-loop simulations show that for the same antenna configurations, the accuracy of the relative positioning solution can improve up to 40%.

1. Introduction

In the United States, Europe and Japan, there are or have been a number of missions requiring relative positioning between elements of the mission and it is expected that this number will continue to increase [1]. We will start with an overview of the most significant missions using the terms chaser and target. The target is the main satellite and, in formation flying the chaser is positioning itself relative to the target and, in case of rendezvous the chaser is approaching the target.

The very first mission to use GNSS (GPS) signals for relative navigation in space was ETS-7 [2]. The ETS-7 experiment used four space qualified L1 GPS receivers: two redundant receivers on each sub-satellite. Recent transport missions to the International Space Station (ISS) utilizing a rendezvous with GPS were performed by the ATV of Europe, and the Japanese HTV. The European PRISMA mission is planned for the near future to demonstrate formation flying techniques in space [3]. Delft University of Technology and the German space agency DLR showed results using orbital data from the GRACE formation where mm level accuracy (1-dimensional) for relative positioning were obtained [4].

If satellites have a number of antennas in a typical configuration as is shown in Fig. 1, GNSS can be used to determine the attitude besides the relative position. In general three antennas are required, and four antennas are common, for platforms using GNSS for full attitude

* Corresponding author. Tel.: +31 15 27 82847; fax: +31 15 27 83711.
E-mail addresses: P.J.Buist@tudelft.nl, pjjbuist@hotmail.com (P.J. Buist).
URL: http://www.lr.tudelft.nl/mgp (P.J. Buist).

0094-5765/$ - see front matter © 2010 Elsevier Ltd. All rights reserved.
doi:10.1016/j.actaastro.2010.09.027

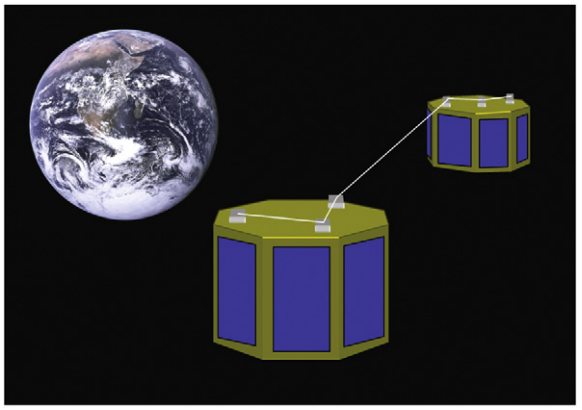

Fig. 1. Artist impression of two satellites with GNSS multi-antenna configurations flying in formation.

Table 1
Number of antennas on the individual elements of missions utilizing GNSS-based relative positioning.

Mission	Number of antennas at	
	Target	Chaser
ETS7	1	2
GRACE	1	1
ATV	>4(*ISS*)	1
HTV	>4(*ISS*)	3
PRISMA	1	1
TR-X/TD-X	3	3
FFAST	3	1

determination [5]. This attitude solution can enhance the relative positioning between satellites as we will show in this paper. A number of missions, applying GNSS for relative positioning between elements, have more than one antenna on the individual satellites. For the ETS-7 mission, the chaser satellite had two antennas and the target satellite one, and therefore this configuration of three antennas made a two baseline system [6]. The ATV has two redundant receivers but they are not used at the same time [7], therefore only one antenna is used for relative positioning [8]. The ISS has a number of receivers [9–11] with one of them connected to a number of antennas being applied for attitude determination [12]. The HTV has three redundant *Space Integrated GPS/INS* (SIGI) units and the Japanese Experiment Module on the ISS has another two of these units, with each SIGI having its own antenna [13]. Other examples of missions with multiple antennas at some of their elements are Terrasar-X (TR-X) and TanDEM-X (TD-X) [14], and FFAST [15]. On the TR-X/TD-X mission two receivers are used on each satellite, with one receiver connected to two antennas. For FFAST, GPS will also be applied for attitude determination of the detector spacecraft and therefore this satellite will have three antennas. The PRISMA mission has two antennas at opposite sides of each spacecraft. During the flight the spacecraft will select automatically the antenna to be used [16]. The number of antennas on the elements of the discussed missions are summarized in Table 1.

We will conclude this introduction with some general remarks on trends in space mission design. Currently there is a trend in space mission design towards payload distribution where one satellite, integrally carrying all payload, is replaced by a cluster or swarm of smaller satellites [1]. The function of the former integrated satellite is distributed over the elements of the cluster, with most often a requirement to know the relative positions and orientations of the elements. If this information is being provided by GNSS in an integrated approach this could result in more flexible mission and lower cost. In this contribution we will develop such an integrated approach to enhance relative positioning.

2. Modelling

As described in the previous section, there are formation flying missions with more than one GNSS antenna on each platform. Up until now the observations from all these antennas are not applied for precise relative positioning, the research topic of this contribution. This paper introduces a method for multi-antenna ambiguity resolution for constrained and unconstrained baselines and describes the method mathematically. Unconstrained baselines are baselines for which a-priori information about the length is not available and constrained baselines are baselines for which the length is known and constant.

2.1. Unconstrained model

Most GNSS receivers make use of two types of observations: pseudo range and carrier phase. The pseudo range observations typically have an accuracy of decimeters, whereas carrier phase observations have accuracies down to millimeter level. The double difference (DD) observation equations can be written for a single baseline as a system of linearized observation equations [17]:

$$E(y) = Az + Gb, \quad D(y) = Q_{yy} \tag{1}$$

Where $E(y)$ is the mean or the expected value and $D(y)$ is the variance or dispersion of y. y is the vector of observed minus computed DD carrier phases and/or code observations, z is the unknown vector of ambiguities of the order n expressed in cycles rather than range to maintain their integer character. b is the baseline vector, whose length is generally known for applications where we consider the distance between antennas at the same platform. G is the geometry matrix containing normalized line-of-sight vectors, A is a design matrix that links the data vector to the unknown vector z. In this paper the assumption is made that the antennas are close to each other and thus that atmospheric effects can be neglected. The variance matrix of y is given by the positive definite matrix Q_{yy}, which is assumed to be known. In our notation we will make use of the weighted squared norm $\|..\|^2_{Q_{yy}} = (..)^T Q_{yy}^{-1}(..)$.

The set of linear observation equations is solved by applying the well-known integer least-squares principle [18]:

$$\min_{z\in\mathbb{Z}^n, b\in\mathbb{R}^3} \|y - Az - Gb\|^2_{Q_{yy}} \tag{2}$$

for which the solution can be obtained from the following three steps:

(1) First the so-called float solution $\hat{z}$ and $\hat{b}$ is obtained, i.e. the least-squares solution disregarding the integer nature of the ambiguities. The variance–covariance (or v–c) matrix of this solution is derived as

$$\begin{bmatrix} Q_{\hat{z}\hat{z}} & Q_{\hat{z}\hat{b}} \\ Q_{\hat{b}\hat{z}} & Q_{\hat{b}\hat{b}} \end{bmatrix} = [(A,G)^T Q_{yy}^{-1}(A,G)]^{-1} \quad (3)$$

Furthermore, we introduce the v–c matrix for $\hat{b}(z)$, the least-squares solution for b assuming that z is known, as $Q_{\hat{b}(z)\hat{b}(z)} = Q_{\hat{b}\hat{b}} - Q_{\hat{b}\hat{z}} Q_{\hat{z}\hat{z}}^{-1} Q_{\hat{z}\hat{b}}$.

(2) We solve the vector of integer least-squares estimates of the ambiguities $\check{z}$:

$$\check{z} = \arg\left(\min_{z\in\mathbb{Z}^n} \|\hat{z}-z\|^2_{Q_{\hat{z}\hat{z}}} \right) \quad (4)$$

where $\check{z}$ is the vector of integers that minimizes the term within the brackets (arg or *argument*). This integer ambiguity vector is estimated by means of an extensive search for the integer vector which minimizes the distance with respect to the float solution in the metric of the v–c matrix of the ambiguities. This step is performed by the LAMBDA method [18].

(3) The fixed baseline solution is obtained using the estimated integer ambiguities: $\check{b} = \hat{b}(\check{z}) = \hat{b} - Q_{\hat{b}\hat{z}} Q_{\hat{z}\hat{z}}^{-1} (\hat{z}-\check{z})$.

In order to evaluate and validate the fixed solution, the associated mixed integer parameter distributions must be used for testing and success rate computations [19–21].

2.2. Constrained model

For baselines whose length $\|b\| = l$ is known, the minimization problem is reformulated as

$$\min_{z\in\mathbb{Z}^n, b\in\mathbb{R}^3, \|b\|=l} \|y - Az - Gb\|^2_{Q_{yy}} \quad (5)$$

This solution follows the same steps as above, with the exception that the search for the integer vector is now done with the constrained (C-) LAMBDA method [22–25]:

$$\check{z} = \arg\left(\min_{z\in\mathbb{Z}^n} (\|\hat{z}-z\|^2_{Q_{\hat{z}\hat{z}}} + \|\hat{b}(z)-\check{b}(z)\|^2_{Q_{\hat{b}(z)\hat{b}(z)}}) \right) \quad (6)$$

where $\check{b}(z)$ is the fixed solution for b, assuming that z is known: $\check{b}(z) = \arg\left(\min_{b\in\mathbb{R}^3, \|b\|=l} \|\hat{b}(z)-b\|^2_{Q_{\hat{b}(z)\hat{b}(z)}} \right)$. This method integrates the nonlinear baseline constraint into the search for the integer minimizer. The C-LAMBDA method is a nontrivial modification of the LAMBDA method. It is shown in [22] how to perform such a search in an efficient way. The constrained method achieves higher performance due to the rigorous inclusion into the integer estimation process of the nonlinear constraint, as given by the known distance between the GNSS antennas.

3. Baseline constrained multi-antenna ambiguity resolution

Precise relative positioning of two moving platforms usually requires dual-frequency phase data, whereas – due to the baseline length constraints – single-frequency phase data may suffice for the precise determination of platform attitudes [23,26,27]. In this contribution we will combine the two problems and apply a single processing strategy for solving them. First, we will introduce a multi-antenna configuration on two separate platforms. The basic theory for a three- and four-antenna configuration, situated at two platforms with at most two antennas on each platform, was developed in [28,29]. In these publications the performance of the method was confirmed with simulated data and a simple field experiment utilizing three antennas on a single platform. In this contribution we will extend the method to be applicable with more antennas. We will show the theoretical improvement achievable as a function of the number of antennas on each platform. We make use of a solution for individual constrained baselines that is suboptimal as not all information available is applied, namely the relative orientation of the baselines. This limitation could be overcome by the multivariate constrained LAMBDA method described in [30–32]. However, we will use the solution for individual baselines in a sequential order as a first step to prove the concept of the integrated approach in what is called vectorial bootstrapping.

3.1. Multi-baseline setup

As is shown in Fig. 2, in our multi-antenna configuration the number of antennas at a single platform is $N+1$ and the number of independent baselines is therefore N.

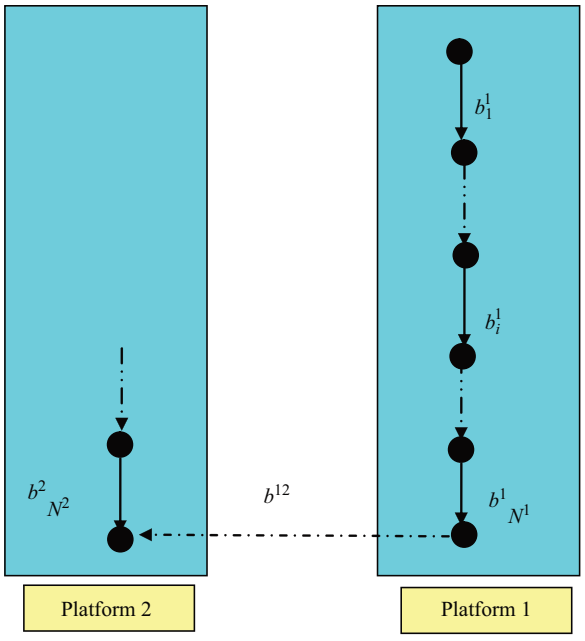

Fig. 2. Illustration of the multi-antenna configuration on two platforms.

The first constrained baseline on platform 1 is called baseline b_1 and the last baseline b_N. In order to distinguish between antennas and baselines at different platforms we introduce a superscript indicating the platform, e.g. the first constrained baseline on platform 1 is written as b_1^1 in Fig. 2. The unconstrained baseline connecting the two platforms is then written as b^{12}. For simplicity we show the baselines in Fig. 2 as aligned, but generally a different antenna configuration will be used for attitude determination. For compactness in this theoretical discussion the design matrices A and G and the variance–covariance matrix Q_{yy} are assumed to be identical. This is a reasonable assumption as we make use of only L1 observations and the antennas are assumed to be sufficiently close, so that the relative antenna-satellite geometry may be considered the same for all antennas. In our software implementation, the design matrices are only assumed to be identical if they apply to antennas at the same platform. Next we will introduce a matrix formulation for this multi-baseline problem based on [30]. We will make use of a $2n \times N$ data matrix $Y=[y_1,\ldots,y_N]$ where each column corresponds to one baseline, an $n \times N$ matrix $Z=[z_1,\ldots,z_N]$ of N DD integer ambiguity vectors and a $3 \times N$ matrix $B=[b_1,\ldots,b_N]$ of N unknown baseline vectors. The linear multiple antenna model can be formulated as

$$E(Y) = AZ + GB \tag{7}$$

In order to apply the integer least-squares principle to Eq. (7), we will write this equation in the form of Eq. (1) using the vec-operator. The vec-operator is a linear transformation which transforms a matrix into a vector by stacking the columns of the matrix one underneath the other (see Appendix A). Application of the vec-operator and the Kronecker product $\otimes$ gives

$$\begin{aligned} E(vec(Y)) &= (I_N \otimes A)vec(Z) + (I_N \otimes G)vec(B) \\ D(vec(Y)) &= P_N \otimes Q_{yy} \end{aligned} \tag{8}$$

To describe the dispersion of the observations at all baselines we make use of $P \otimes Q_{yy}$, where matrix P takes care of the correlation that follows from the fact that consecutive baselines have one antenna in common. For a discussion on matrix P, we refer to [28,29]. In this section we will apply an $N \times N$ tridiagonal matrix:

$$P_N = \begin{bmatrix} 1 & -\frac{1}{2} & 0 & \cdots & 0 \\ -\frac{1}{2} & 1 & -\frac{1}{2} & & \vdots \\ 0 & -\frac{1}{2} & 1 & \ddots & 0 \\ \vdots & & \ddots & \ddots & -\frac{1}{2} \\ 0 & \cdots & 0 & -\frac{1}{2} & 1 \end{bmatrix} \tag{9}$$

The least-squares solution and corresponding v–c matrix of the N+1-antenna configuration, which includes the unconstrained baseline b^{12} to the other platform, can be given as [29]

$$\begin{bmatrix} vec(\hat{Z}^1) \\ \hat{z}^{12} \\ vec(\hat{B}^1) \\ \hat{b}^{12} \end{bmatrix} = \begin{bmatrix} I_{N^1+1} \otimes (Q_{\hat{z}\hat{z}} A^T Q_{yy}^{-1} + Q_{\hat{z}\hat{b}} G^T Q_{yy}^{-1}) \\ I_{N^1+1} \otimes (Q_{\hat{b}\hat{z}} A^T Q_{yy}^{-1} + Q_{\hat{b}\hat{b}} G^T Q_{yy}^{-1}) \end{bmatrix} \begin{bmatrix} vec(Y^1) \\ y^{12} \end{bmatrix}$$

$$D\begin{bmatrix} vec(\hat{Z}^1) \\ \hat{z}^{12} \\ vec(\hat{B}^1) \\ \hat{b}^{12} \end{bmatrix} = \begin{bmatrix} P_{N+1} \otimes Q_{\hat{z}\hat{z}} & P_{N+1} \otimes Q_{\hat{z}\hat{b}} \\ P_{N+1} \otimes Q_{\hat{b}\hat{z}} & P_{N+1} \otimes Q_{\hat{b}\hat{b}} \end{bmatrix} \tag{10}$$

This shows that $\hat{z}_i$ and $\hat{b}_i$ are solely determined by the DD observation vector of the corresponding antenna pair, that is y_i. Thus parallel processing is possible for the float solution.

3.2. Integer least-squares for an N+1 antenna configuration

In order to obtain the unknown parameters we need to solve the following minimization problem for a single platform with N constrained baselines, and a single unconstrained baseline to an antenna at another platform.

$$\begin{aligned} &\min_{\substack{[Z^1,z^{12}]\in\mathbb{Z}^{n\times(N^1+1)} \\ [B^1,b^{12}]\in\mathbb{R}^{3\times N^1} \\ \|b_j^1\|=l_j^1,\, j=1\ldots N^1}} \left\| \begin{matrix} vec(Y^1)-(I_N\otimes A)vec(Z^1)-(I_N\otimes G)vec(B^1) \\ y^{12}-Az^{12}-Bb^{12} \end{matrix} \right\|^2_{P_{N+1}\otimes Q_{yy}} \\ &= \left\| \begin{matrix} vec(\hat{E}^1) \\ \hat{e}^{12} \end{matrix} \right\|^2_{P_{N+1}\otimes Q_{yy}} + \min_{\substack{[Z^1,z^{12}]\in\mathbb{Z}^{n\times(N^1+1)} \\ [B^1,b^{12}]\in\mathbb{R}^{3\times N^1} \\ \|b_j^1\|=l_j^1,\, j=1\ldots N^1}} \left(\left\| \begin{matrix} vec(\hat{Z}^1-Z^1) \\ \hat{z}^{12}-z^{12} \end{matrix} \right\|^2_{P_{N+1}\otimes Q_{\hat{z}\hat{z}}} \right. \\ &\left. + \left\| \begin{matrix} vec(\hat{B}^1(Z^1,z^{12})-B^1) \\ \hat{b}^{12}(Z^1,z^{12})-b^{12} \end{matrix} \right\|^2_{P_{N+1}\otimes Q_{\hat{b}(z)\hat{b}(z)}} \right) \end{aligned} \tag{11}$$

where $\hat{e} = y - A\hat{z} - B\hat{b}$ is the least-squares residual vector of the float solution $\hat{z},\hat{b}$ and $\hat{E} = Y - A\hat{Z} - G\hat{B}$ is the least-squares residual matrix in which $\hat{Z}$ and $\hat{B}$ are the least-squares estimators of Z and B, respectively, without taking the integer and baseline length constraints into account.

The ambiguity-constrained baseline solution with associated variance–covariance matrix is given as

$$\begin{aligned} &\begin{bmatrix} vec(\hat{B}^1(Z^1,z^{12})-B^1) \\ \hat{b}^{12}(Z^1,z^{12})-b^{12} \end{bmatrix} \\ &= \begin{bmatrix} vec(\hat{B}^1) \\ \hat{b}^{12} \end{bmatrix} - (P_{N+1}\otimes Q_{\hat{b}\hat{z}})(P_{N+1}\otimes Q_{\hat{z}\hat{z}})^{-1} \begin{bmatrix} vec(\hat{Z}^1-Z^1) \\ \hat{z}^{12}-z^{12} \end{bmatrix} \\ &= \begin{bmatrix} vec(\hat{B}^1) \\ \hat{b}^{12} \end{bmatrix} - I_{N^1+1}\otimes Q_{\hat{b}\hat{z}}Q_{\hat{z}\hat{z}}^{-1} \begin{bmatrix} vec(\hat{Z}^1-Z^1) \\ \hat{z}^{12}-z^{12} \end{bmatrix} \\ &= \begin{bmatrix} vec(\hat{B}^1(Z^1)-B^1) \\ \hat{b}^{12}(z^{12})-b^{12} \end{bmatrix} \\ &D\begin{bmatrix} vec(\hat{B}^1(Z^1,z^{12})-B^1) \\ \hat{b}^{12}(Z^1,z^{12})-b^{12} \end{bmatrix} = P_{N+1}\otimes Q_{\hat{b}(z)\hat{b}(z)} \end{aligned} \tag{12}$$

As was demonstrated in [28,29], it follows that each conditional baseline depends only on its own ambiguity

vector, thus knowledge about z_i^1 does not contribute directly to the subsequent conditional baseline estimates $\hat{b}_{i+1}^1(z_{i+1}^1)$ and $\hat{b}^{12}(z^{12})$. Therefore the last term of Eq. (11) is equal to $\left\| \begin{matrix} vec(\hat{B}^1(Z^1)-B^1) \\ \hat{b}^{12}(z^{12})-b^{12} \end{matrix} \right\|^2_{P_{N+1}\otimes Q_{\hat{b}(z)\hat{b}(z)}}$ and can be decomposed as

$$\left\| \begin{matrix} vec(\hat{B}^1(Z^1)-B^1) \\ \hat{b}^{12}(z^{12})-b^{12} \end{matrix} \right\|^2_{P_{N+1}\otimes Q_{\hat{b}(z)\hat{b}(z)}} = \|\hat{b}_1^1(z_1^1)-b_1^1\|^2_{Q_{\hat{b}(z)\hat{b}(z)}} + \sum_{i=2}^{N^1} \|\hat{b}_i^1(z_i^1,b_I^1)-b_i^1\|^2_{X_i^1 Q_{\hat{b}(z)\hat{b}(z)}} + \|\hat{b}^{12}(z^{12},b_{N^1}^1,\ldots,b_1^1)-b^{12}\|^2_{X_{N^1+1}^1 Q_{\hat{b}(z)\hat{b}(z)}} \quad (13)$$

with $\hat{b}_i^1(z_i^1,b_I^1)$ is the ith baseline conditioned on the ambiguity z_i and the previous baselines $b_I^1 = \cup_{j=1}^{i-1} b_j^1$.

As explained in Appendix B and using the relations we have found we can write the scaling factor X for the v–c matrix for the i-th baseline as

$$X_1^1 = 1$$

For $i = 1,\ldots,N^1$

$$X_{i+1}^1 = \frac{i+2}{2(i+1)} \quad (14)$$

We observe that the scaling factor for the ith baseline can be calculated directly, i.e. it is not necessary to do this sequentially.

The integer least-squares solution becomes for this N^1 constrained and one unconstrained baseline configuration:

$$\begin{bmatrix} vec(\check{Z}^1) \\ \check{z}^{12} \end{bmatrix} = \arg\min_{z\in\mathbb{Z}^{n\times(N^1+1)}} \left(\|\hat{z}_1^1-z_1^1\|^2_{Q_{\hat{z}\hat{z}}} + \|\hat{b}_1^1(z_1^1)-\check{b}_1^1(z_1^1)\|^2_{Q_{\hat{b}(z)\hat{b}(z)}} + \sum_{i=2}^{N^1} \left(\|\hat{z}_i^1(z_I^1)-z_i^1\|^2_{X_i^1 Q_{\hat{z}\hat{z}}} + \|\hat{b}_i^1(z_i^1,b_I^1)-\check{b}_i^1(z_i^1,b_I^1)\|^2_{X_i^1 Q_{\hat{b}(z)\hat{b}(z)}} \right) + \|\hat{z}^{12}\left(z_{N^1}^1,\ldots,z_1^1\right)-z^{12}\|^2_{X_{N^1+1}^1 Q_{\hat{z}\hat{z}}} \right) \quad (15)$$

for which $z_I^1 = \cup_{j=1}^{i-1} z_j^1$ and

$$\|\hat{b}_1^1(z_1^1)-\check{b}_1^1(z_1^1)\|^2_{Q_{\hat{b}(z)\hat{b}(z)}} + \sum_{i=2}^{N^1} \|\hat{b}_i^1(z_i^1,b_I^1)-\check{b}_i^1(z_i^1,b_I^1)\|^2_{X_i^1 Q_{\hat{b}(z)\hat{b}(z)}} = \min_{\substack{\|b_j^1\|=l_j^1 \\ j=1,\ldots,N^1}} \left(\|\hat{b}_1^1(z_1^1)-b_1^1\|^2_{Q_{\hat{b}(z)\hat{b}(z)}} + \sum_{i=2}^{N^1} \|\hat{b}_i^1(z_i^1,b_I^1)-b_i^1\|^2_{X_i^1 Q_{\hat{b}(z)\hat{b}(z)}} \right)$$

An approximation of the integer least-squares solution can be obtained by solving the baselines sequentially where the solution of baseline i is applied on the next, as if the correlation between baselines would be absent [29]. The result is a vectorial bootstrapping approach in which we first solve the ambiguities on the constrained baselines and finally apply the found ambiguity vector in the solution of the unconstrained baseline. This solution is then given as

$$\check{z}_1^1 = \arg\min_{z_1^1\in\mathbb{Z}^n} \left(\|\hat{z}_1^1-z_1^1\|^2_{Q_{\hat{z}\hat{z}}} + \min_{\|b_1^1\|=l_1^1} \left(\|\hat{b}_1^1(z_1)-b_1^1\|^2_{Q_{\hat{b}(z)\hat{b}(z)}} \right) \right)$$

$$\check{z}_2^1 = \arg\min_{z_2^1\in\mathbb{Z}^n} \left(\|\hat{z}_2^1(\check{z}_1^1)-z_2^1\|^2_{\frac{3}{4}Q_{\hat{z}\hat{z}}} + \min_{\|b_2^1\|=l_2^1} \left(\|\hat{b}_2^1(z_2^1)-b_2^1\|^2_{\frac{3}{4}Q_{\hat{b}(z)\hat{b}(z)}} \right) \right)$$

$$\vdots$$

$$\check{z}_{N^1}^1 = \arg\min_{z_{N^1}^1\in\mathbb{Z}^n} \left(\|\hat{z}_{N^1}^1(\check{z}_I^1)-z_{N^1}^1\|^2_{X_{N^1}^1 Q_{\hat{z}\hat{z}}} + \min_{\|b_{N^1}^1\|=l_{N^1}^1} \left(\|\hat{b}_{N^1}^1(z_{N^1}^1)-b_{N^1}^1\|^2_{X_{N^1}^1 Q_{\hat{b}(z)\hat{b}(z)}} \right) \right)$$

$$\check{z}^{12} = \arg\min_{z^{12}\in\mathbb{Z}^n} \left(\|\hat{z}^{12}(\check{z}_{N^1}^1,\ldots,\check{z}_1^1)-z^{12}\|^2_{X_{N^1+1}^1 Q_{\hat{z}\hat{z}}} \right)$$

With the constraint on the baseline and the ambiguities, the conditional solution of the baselines becomes

$$\check{b}_1^1 = \arg\min_{\|b_1^1\|=l_1^1} \left(\|\hat{b}_1^1(\check{z}_1)-b_1^1\|^2_{Q_{\hat{b}(z)\hat{b}(z)}} \right)$$

$$\check{b}_2^1 = \hat{b}_2^1(\check{z}_2^1,\check{b}_1^1)$$

$$\vdots$$

$$\check{b}_{N^1}^1 = \hat{b}_{N^1}^1(\check{z}_{N^1}^1,\check{b}_I^1)$$

$$\check{b}^{12} = \hat{b}^{12}(\check{z}^{12},\check{b}_{N^1}^1,\ldots,\check{b}_1^1)$$

with for example for the solution of the second constrained baseline conditioned on its ambiguity vector and the previous baseline [29]:

$$\hat{b}_2^1(\check{z}_2^1,\check{b}_1^1) = \arg\min_{\|b_2^1\|=l_2^1} \left(\|\hat{b}_2^1(\check{z}_2^1)-b_2^1\|^2_{Q_{\hat{b}(z)\hat{b}(z)}} \right) + \frac{1}{2}(\hat{b}_1^1(\check{z}_1^1)-\check{b}_1^1) \quad (16)$$

From Eq. (13) and (15) it is clear that the reduction on the dispersion (i.e. the scaling factor X) on the baseline and ambiguity vectors is the same. This relationship is consistent with the scaling factors obtained in [29]. The first two rows in Table 2 shows this scaling factor of $Q_{\hat{z}\hat{z}}$ and $Q_{\hat{b}(z)\hat{b}(z)}$ for a platform with up to 11 antennas (i.e. 10 baselines). For convenience we introduce C, which indicates the total number of constrained baselines in the configuration (here $C=N^1$). As discussed in the Introduction (Section 1), the three- and four-antenna configurations are most relevant for our application and therefore we will investigate the cases C=1, 2, 4 and 6 marked in Table 2 further by simulation in the next section. These cases are shown in Fig. 3.

A similar general formula can be derived if the unconstrained baseline between the two platforms is constrained by constrained baselines at both sides [29]. Then we can extend this theory to a general model for a multi-antenna configuration at both platforms with N^1 constrained baselines $b_1^1,\ldots,b_{N^1}^1$ at the first platform, N^2 constrained baselines $b_1^2,\ldots,b_{N^2}^2$ at the other platform and

Table 2
Scaling factor for the v–c matrix as a function of the number of constrained baselines, the bold values indicates cases that will be simulated.

#C	1	2	3	4	5	6	7	8	9	10
One side	**3/4**	2/3	5/8	3/5	7/12	4/7	9/16	5/9	11/20	6/11
#C	2	4	6	8	10	12	14	16	18	20
Two side	**1/2**	**1/3**	**1/4**	1/5	1/6	1/7	1/8	1/9	1/10	1/11

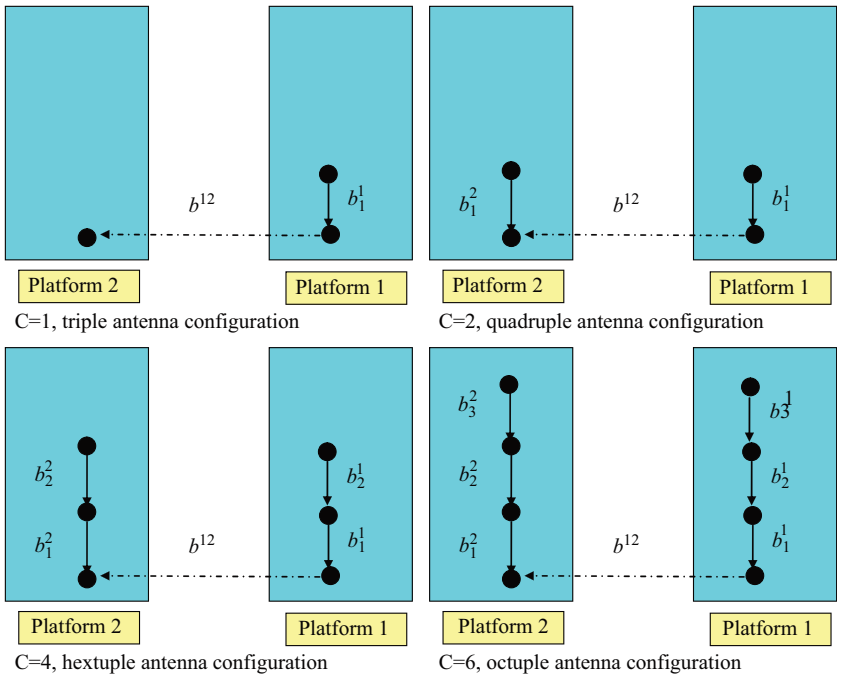

Fig. 3. Definition of two platforms and C antenna configuration.

the unconstrained baseline between both platforms defined as b^{12}. We can write

$$\left\| \begin{matrix} vec(\hat{B}^1(Z^1)-B^1) \\ vec(\hat{B}^2(Z^2)-B^2) \\ \hat{b}^{12}(z^{12})-b^{12} \end{matrix} \right\|^2_{P\otimes Q_{\hat{b}(z)\hat{b}(z)}} = \|\hat{b}_1^1(z_1^1)-b_1^1\|^2_{Q_{\hat{b}(z)\hat{b}(z)}} + \sum_{i=2}^{N^1} \|\hat{b}_i^1(z_i^1,b_i^1)-b_i^1\|^2_{X_i^1 Q_{\hat{b}(z)\hat{b}(z)}} + \|\hat{b}_2^2(z_2^2)-b_2^2\|^2_{Q_{\hat{b}(z)\hat{b}(z)}} + \sum_{i=2}^{N^2} \|\hat{b}_i^2(z_i^2,b_i^2)-b_i^2\|^2_{X_i^2 Q_{\hat{b}(z)\hat{b}(z)}} + \|\hat{b}^{12}(z^{12},b_{N_1}^1,b_{N_2}^2,\ldots,b_1^1,b_1^2)-b^{12}\|^2_{(X^{12}_{N^1N^2})Q_{\hat{b}(z)\hat{b}(z)}} \quad (17)$$

As explained in Appendix B, the scaling factor $X^{12}_{N^1N^2}$ for an unconstrained baseline connected to N^1 constrained baselines at a platform at one side and N^2 constrained baselines at a platform at the other side can be written as

$$X^{12}_{N^1N^2} = \frac{N^1+N^2+2}{2(1+N^1)(1+N^2)}$$
$$C = N^1+N^2 \quad (18)$$

Again we see that the scaling factor can be calculated directly if the number of constrained baselines is known, so it is not necessary to calculate these factors sequentially. If both platforms have the same number of constrained baselines (i.e. $N^1=N^2=N$), we can calculate the scaling factor for the unconstrained baselines between the two platforms as

$$X^{12}_{N^1N^2} = \frac{1}{1+N}$$
$$C = 2N \quad (19)$$

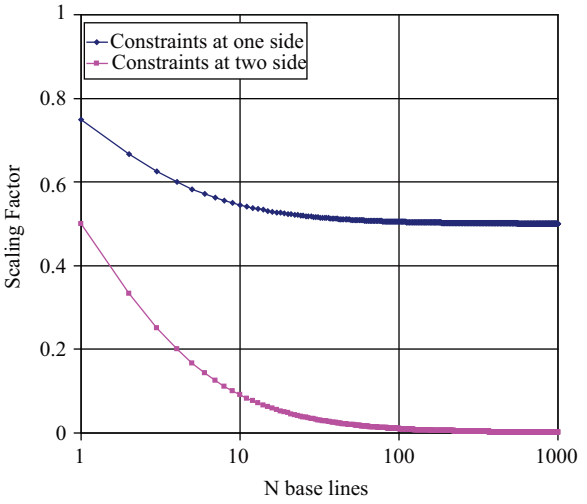

Fig. 4. Theoretical relationship between number of constrained baselines and the scaling factor for the v–c matrix.

The last two rows in Table 2 shows the scaling factor for the v–c matrices of the ambiguity and baseline vectors for the unconstrained baseline between two platforms each with up to 11 antennas. The relation is shown as function of baseline number at one side or at two sides of the unconstrained baseline in Fig. 4. As this figure shows with constraints on one side, the scaling factor approaches $\frac{1}{2}$, and with constraints on both sides this factor will go to a very small value. This means that the improvement is larger with constraints at both sides as the model becomes stronger.

3.3. Discussion

The improvement for the precision of the v–c matrix in the multi-antenna configuration obtained mathematically in Section 3.2 can be explained as follows. First we will discuss the symmetric case of having the same number of antennas $N+1$ on each of the two platforms. We start the discussion with the configuration $C=0$. In this configuration we only have one antenna on each platform and thus no constrained baselines, and one unconstrained baseline between the two platforms. The scaling factor for the v–c matrix of the ambiguity and baseline vectors is then 1. Next we continue with two antennas on each platform (configuration $C=2$) and we assume that the baseline lengths between antenna 1–2 at each platform are known. Assuming that the ambiguities at these baselines can be determined successfully, the baselines b_1^1 and b_1^2 can be determined very precisely (mm-range) and thus almost exactly. But this means that the unconstrained baseline between the antennas 1 at both platforms can also be estimated from the unconstrained baseline between the antennas 2 at both platforms: $b_1^{12}=b_2^{12}+b_1^1-b_1^2$, where $b_1^1-b_1^2$ is known precisely. Hence, we now have observed the 'same' unconstrained baseline (namely b_1^{12} and b_2^{12} in Fig. 5) twice. Thus the variance of the baseline estimate will improve by a factor 1/2. This explanation can be extended to a larger number of constrained baselines at each platform (Fig. 6) but also for the non-symmetric case with a different number of antennas at each platform. Of course for real applications, even for a very large number of baselines, the scaling factor will not become zero as there are remaining biases and errors not included in our model (e.g. absolute positioning errors, influence of ionosphere and multipath), but the improvement is

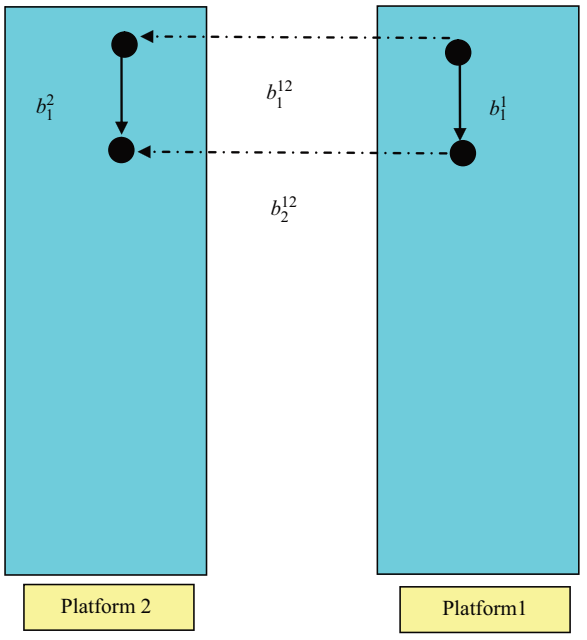

Fig. 5. Definition of unconstrained baselines for the two platforms with two constrained baselines.

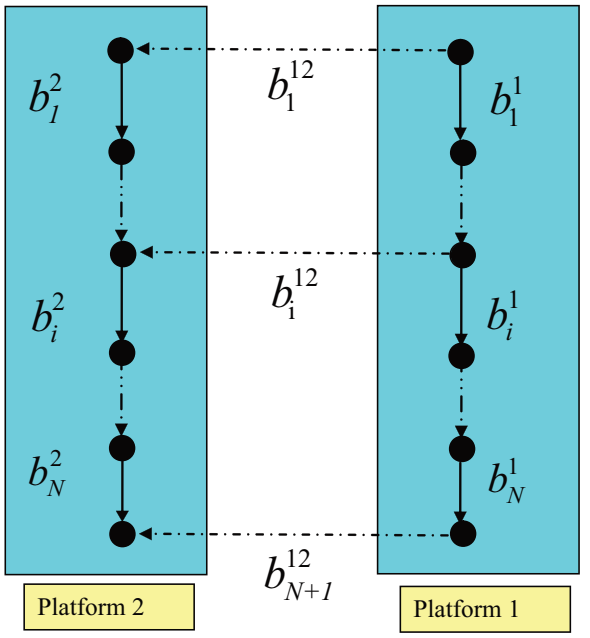

Fig. 6. Definition of unconstrained baselines for the two platforms with C constrained baselines

evident. Another assumption is that we can solve the ambiguities on the constrained baselines with a success rate of close to 100% (a failure rate close to 0%) which seems feasible as was demonstrated in [23,26], especially if we include the geometry of the antenna placement [32].

4. Spacecraft mission

The integrated approach developed in Section 3 is generally applicable to multi-spacecraft missions where GNSS-attitude determination is applied in combination with GNSS-based relative positioning between the elements of the mission. In order to investigate the performance of the proposed integrated approach, we analyze first the empirical failure rates using simulated data. In the second part of this section we analyze the integrated approach using hardware-in-the-loop simulations. In these experiments we will make use of two GPS receivers on two spacecraft and we investigate both empirical success rates and the accuracy of the unconstrained baseline solution. In both software and hardware simulations, we will investigate the most challenging application of single epoch, single frequency ambiguity resolution.

4.1. Software simulation setup

Table 3 summarizes the conditions of the simulations used to investigate the performance of the proposed integrated approach. Utilizing the VISUAL software [33], based on the location of the receivers and an actual GPS constellation, the design matrices of the model are formed. Assuming different noise levels on the undifferenced phase (from 1 to 3 mm) and undifferenced code

Table 3
Software simulation specification.

C	0, 1, 2, 4 and 6
Frequency	L1
Number of satellites	5–6–7–8
Undifferenced code noise σ_p (cm)	30–15–5
Undifferenced phase noise σ_ϕ (mm)	3–1
Baseline length $\|\|b_i^1\|\| = \|\|b_i^2\|\| = l_i$	2.0 m
$\|\|b^{12}\|\|$	150.0 m
Epochs simulated	10^5

Table 4
Orbit specification for the Proba-3 spacecraft.

Orbital period	$\pm$24.1 h
Apogee (altitude)	77,578 (71,200) km
Perigee (altitude)	7,178 (800) km
Inclination	17.8°
Mean anomaly at start of simulation	352°
Nominal ISD	0.150 km

(from 5 to 30 cm) data, a set of 10^5 data was generated; then each simulation was repeated for different number of satellites varying between 5 and 8. The distance $\|\|b^{12}\|\|$ between the main antennas on the two spacecraft is set to 150 m, but this length is not used by the algorithms in Section 5.1.

4.2. Hardware-in-the-loop simulation setup

In our experiment we will make use of two PolaRx2@ receivers [34]. Both satellites have, in addition to the master antenna, two single frequency auxiliary antennas. We will simulate a scenario with the orbital parameters of the Proba-3 mission as shown in Table 4 and a nominal inter-satellite distance (ISD) of 150 m [35]. Again this length is not used by the algorithms in the analyzes described in the next section. As is shown in Fig. 7, the target is flying ahead of the chaser spacecraft (SC). The figure also shows an orbit of a GPS satellite with its transmission pattern directed towards the earth. For the Proba-3 scenario only the part of orbit where the satellites are below the GPS constellation will be simulated (indicated in Fig. 7), as the PolaRx2@ receivers are not modified for an orbit higher than the GPS constellation. According to [35], this matches well with the real mission requirements as the relative GPS equipment will be used during the period where the satellites are below 5000 km. Fig. 8 shows the altitude and velocity of the two spacecraft as a function of simulation time. The velocity of the satellites passing through the perigee is about 9.6 km/s or 34,500 km/hr Both spacecraft are simulated with an earth pointing orientation, and thus rotating around the heading direction.

In Fig. 9 the simulation setup at the ESTEC navigation laboratory is shown, consisting of one Spirent GPS simulator (4760) with three RF outputs and two Septentrio Polarx2@ receivers, adjusted to acquire and track the GPS signals in a LEO environment. More information about the test setup

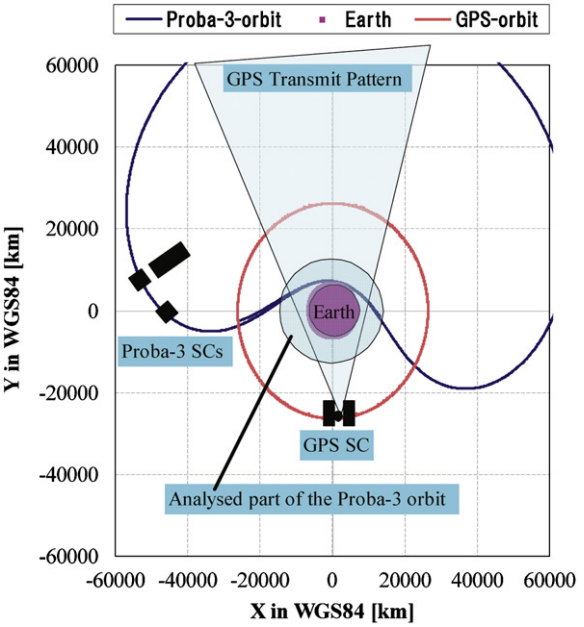

Fig. 7. Orbits of Proba-3 and GPS spacecraft (SC).

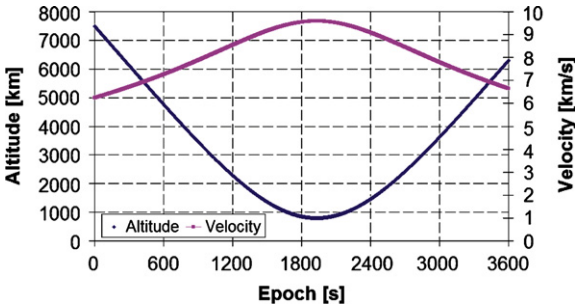

Fig. 8. Altitude and velocity vs. simulation time.

can be found in [35]. We will use the data collected in this set-up to confirm the results of the software simulations described in Section 4.1.

5. Experimental results

5.1. Software simulations

In this section we will analyze the relative positioning result as part of the integrated approach for the antenna configurations in Fig. 3. The results are presented in Fig. 10, which contains empirical failure rates as a function of the number of tracked satellites (N_{SV}) and the phase and code noise (σ_ϕ,σ_p). The unconstrained baseline b^{12} is presented as standalone (C=0) and as part of the integrated solution using a single constrained baseline (C=1) and using two, four or six constrained baselines (C=2, 4 and 6). For the unconstrained baseline in Fig. 10 we observe that the integrated approach has a better performance than standalone. The improvement is up to 13% using a single constrained baseline (C=1), up to

Fig. 9. GPS simulator and receivers.

30% using two constrained baselines (C=2), 43% using four constrained baselines (C=4), and 52% using six constrained baselines (C=6) with a larger improvement for weaker GNSS models.

The probability of obtaining the correct integer value increases, thus the probability of failure decreases, as the precision of $\hat{z}$ improves. For the unconstrained baseline in the quadruple antenna configuration (case C=2 in Fig. 10) we observe a lower failure rate than for the same baseline in the triple antenna configuration (C=1), which is as expected as the variance–covariance matrix is scaled with $\frac{1}{2}$ and $\frac{3}{4}$, respectively, of the original $Q_{\hat{z}\hat{z}}$ of the standalone solution. The unconstrained baseline in, respectively, the hextuple and octuple antenna configuration is scaled with $\frac{1}{3}$ and $\frac{1}{4}$. Therefore we can say that the larger number of constrained baselines in an antenna configuration results in a stronger model.

Another important result is that the availability of a fixed solution for the unconstrained baseline will increase remarkably for the integrated approach compared with standalone. Normally only if the upper bound of the failure rate is lower than a certain threshold an attempt will be made to fix the ambiguities. In Fig. 10, a threshold for the failure rate of 5% is indicated with a bold red line.

5.2. Hardware-in-the-loop simulations

As a last step we analyze the failure rate for the hardware-in-the-loop simulations using a triple antenna configuration at each spacecraft. The number of locked GPS satellites at each of the three antennas on both the Proba-3 spacecraft are shown in Fig. 11. A so called cold start is used for these receivers and in the figures we observe that it takes longer at the first spacecraft to initialize. We start our analysis if more than four GPS satellites are locked at both spacecraft. For the attitude determination result at both platforms, we obtain an empirical success rate for single epoch ambiguity resolution of 100%, so the failure rate is 0%.

Empirical ambiguity failure rates for the unconstrained baseline between the spacecraft are shown in Table 5. The decrease in failure rate from 15% to 9% for the unconstrained baselines in this hardware-in-the-loop experiment is in line with our expectation from the theory developed in the previous sections and the simulation results presented in Fig. 10.

The single epoch relative positioning solutions (C=0 and 4) for the hardware-in-the-loop test are shown in Fig. 12. From the figure it is clear that the integrated solution is more accurate.

Table 5 also contains the standard deviation of the baseline estimates. Here we observe, again in line with the theory developed in Section 3.2, that the accuracy of the baseline estimate increases if more constrained baselines are included in the integrated solution. For example for case C=1, 2 and 4, we know from Table 2, that the standard deviation of the fixed baseline should improve compared to standard LAMBDA with $\sqrt{(\frac{3}{4})} \approx 0.9$, $\sqrt{(\frac{1}{3})} \approx 0.7$ and $\sqrt{(\frac{1}{2})} \approx 0.6$, respectively. If we compare these numbers with the empirical results in Table 5, we observe an improvement as expected of $\frac{1.5}{1.8} \approx 0.8$, $\frac{1.2}{1.8} \approx 0.7$ and $\frac{1.1}{1.8} \approx 0.6$, respectively.

Based on the presented results we conclude that we have demonstrated using hardware-in-the-loop simulations that an integrated approach (i.e. the vectorial bootstrapping approach) can improve both ambiguity resolution and accuracy of the unconstrained baseline between platforms.

6. Conclusions

In this contribution we investigated the possibility to use multi-antenna data, not only for attitude determination, but also to improve the relative positioning between spacecraft in an integrated approach. The method makes use of the following information to determine the relative position and orientation of a multi-antenna system with unconstrained and constrained baselines: the integerness

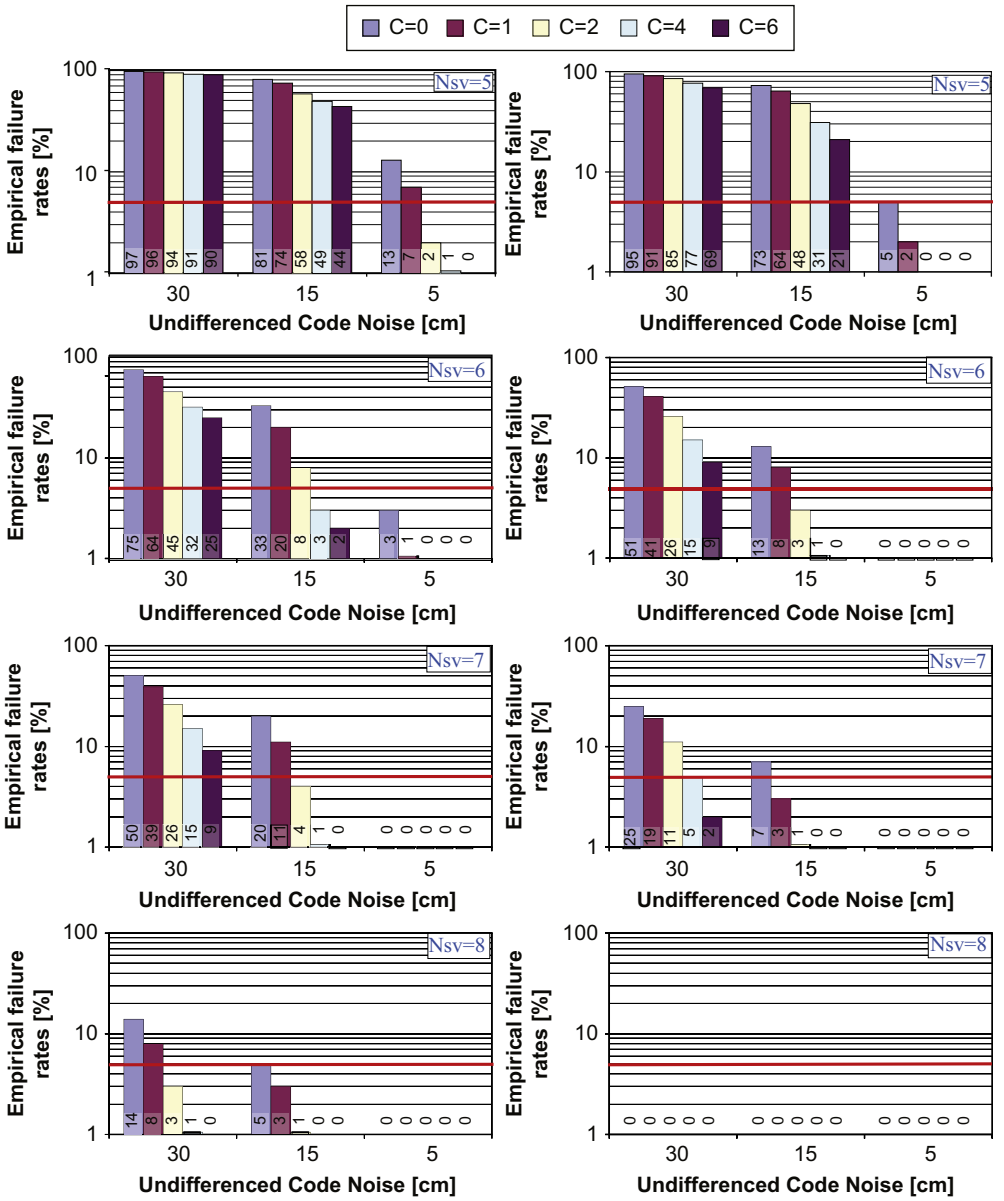

Fig. 10. Single-frequency, single-epoch failure rates for undifferenced carrier noise of 3 mm (left) and 1 mm (right) for the unconstrained baseline using zero (C=0), one (C=1, i.e. triple antenna configuration), two (C=2, i.e. quadruple antenna configuration), four (C=4, i.e. Hextuple antenna configuration) or six (C=6, i.e. Octuple antenna configuration) constrained baselines.

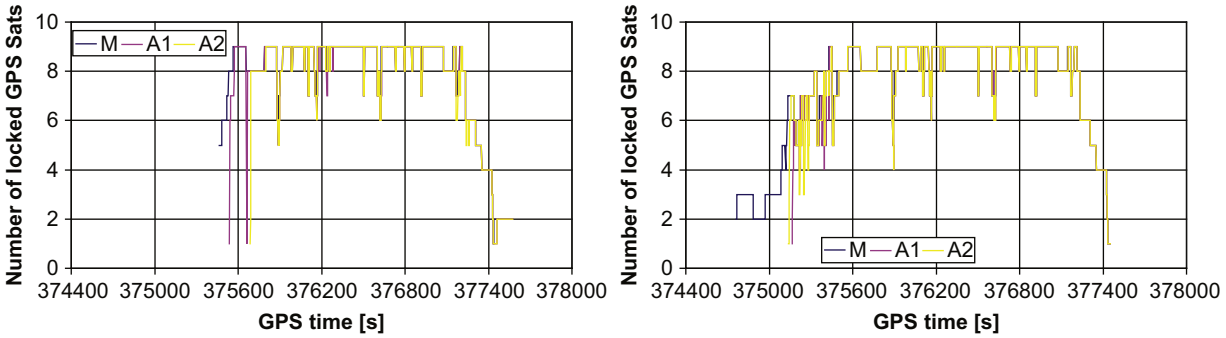

Fig. 11. Number of locked GPS satellites vs. GPS time.

Table 5
Hardware-in-the-loop simulation results: single-frequency, single-epoch failure rates and standard deviation for the unconstrained baseline b^{12} using standard LAMBDA (C=0), and a bootstrapped solution using constrained baselines with C is the total number of constrained baselines at the two spacecraft.

#C	0	1	2	4
Failure rate (%)	0.15	0.11	0.09	0.09
Standard deviation (mm)	1.8	1.5	1.2	1.1

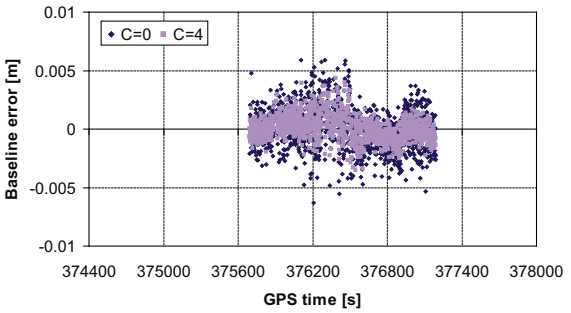

Fig. 12. Baseline error for hardware-in-the-loop test with Proba-3 orbital characteristics, using zero (C=0) and four (C=4) constrained baselines.

of the ambiguities, the relationship between the ambiguities on the different baselines and the known baseline length of the constrained baselines. We showed the theoretical improvement achievable for the unconstrained baseline between the platforms as a function of the number of antennas on each platform, both for ambiguity resolution and accuracy of the baseline solution. The obtained mathematical relationship between the improvement achievable and the number of antennas was verified by software based and hardware-in-the-loop simulations. For these simulations we used missions parameters of the European Proba-3 mission. The software simulations indicated that this approach can improve single epoch ambiguity resolution up to 50% for relative positioning applying the typical antenna configurations for attitude determination. The hardware-in-the-loop simulations show that for the same antenna configurations, the accuracy of the relative positioning solution can improve up to 40%.

Acknowledgements

The GPS simulators and receivers used for the test have been provided by the navigation laboratory of the European Space Agency (ESA-ESTEC). The authors would like to thank the people from this laboratory, especially Alberto Garcia-Rodríguez, Jaron Samson and David Jeménez Banos, for their support. Also the MicroNed-MISAT framework are kindly thanked for their support. Professor Teunissen is the recipient of an Australian Research Council Federation Fellowship (project number FF0883188). This work has also been done in the context of the Australian Space Research Program project: SAR Formation Flying. The research of Sandra Verhagen is supported by the Dutch Technology Foundation STW, applied science division of NWO and the Technology Program of the Ministry of Economic Affairs. All this support is greatly acknowledged.

Appendix A. *vec* Operator

The vec-operator is a linear transformation which transforms a matrix into a vector by stacking the columns of the matrix one underneath the other:

$vec(A)=(a_1^{\mathrm{T}}, a_2^T,\ldots,a_N^T)$.

A property of the vec-operator applied in this contribution is

$$vec(ABC)=(C^T\otimes A)vec(B).$$

Appendix B. Derivation of the scaling factor for the v–c matrix

For convenience we introduce the $(i-1)$-vector q_{i-1} with $-\frac{1}{2}$ as the $(i-1)$th element and zeros otherwise (so $q_{i-1}=[0,\ldots,0,-\frac{1}{2}]$). Here we develop the scaling factor for the v–c matrix if the unconstrained baseline is on one side constrained by one or more constrained baseline. The same discussion can be extended to the case with constrained baselines at both platforms. We will make use of the expression Eq. (20) found in Appendix C for the inverse of the tridiagonal matrix.

Using this notation we can write the ith baseline conditioned on the ambiguity z_i and the previous baselines $b_I=\cup_{j=1}^{i-1} b_j$ as

$$\begin{aligned}\hat{b}_i(z_i,b_I)&=\hat{b}_i(z_i)-q_{i-1}P_{i-1}^{-1}vec(\hat{B}(Z)-B)\\&=\hat{b}_i(z_i)+\tfrac{1}{2}[0,\ldots,0,1]P_{i-1}^{-1}vec(\hat{B}(Z)-B)\end{aligned}$$

and the associated variance–covariance matrix as

$$\begin{aligned}Q_{\hat{b}_i(z_i,b_I)\hat{b}_i(z_i,b_I)}&=Q_{\hat{b}(z)\hat{b}(z)}-q_{i-1}P_{i-1}^{-1}q_{i-1}^TQ_{\hat{b}(z)\hat{b}(z)}\\&=Q_{\hat{b}(z)\hat{b}(z)}-\frac{1}{4}[0,\ldots,0,1]P_{i-1}^{-1}[0,\ldots,0,1]^TQ_{\hat{b}(z)\hat{b}(z)}\\&=\frac{i+2}{2(i+1)}Q_{\hat{b}(z)\hat{b}(z)}\end{aligned}$$

So we observe that the conditional baseline can be calculated from the last column of matrix P_{i-1}^{-1} divided by 2 and the scaling factor from 1 minus the last element of P_{i-1}^{-1} divided by 4.

Appendix C. Inverse of tridiagonal matrix *P*

The inverse of tridiagonal matrices is often found in applied linear algebra, as for example in applications as genetics, finite elements analysis, partial differential equations, signal processing [36]. The analytic expression of the inverse $R(=P^{-1})$ for the tridiagonal matrix P introduced in

this paper was, as far as we know, first published in [37] as

$$r_{ij}=\begin{cases}\dfrac{2j(N+1-i)}{N+1}, & i\geq j\\ \dfrac{2i(N+1-j)}{N+1}, & i<j\end{cases} \tag{20}$$

In [37] this solution was provided without a theoretical proof. In [38] expression (20) was derived, as far as we know, for the first time. For completeness we include another direct proof of the expression in this appendix.

Proof. Consider the jth column of the inverse matrix $R=P^{-1}$:

$$\begin{bmatrix} 1 & -\frac{1}{2} & & & & & & \\ -\frac{1}{2} & 1 & -\frac{1}{2} & & & & & \\ & \ddots & \ddots & \ddots & & & & \\ & & -\frac{1}{2} & 1 & -\frac{1}{2} & & & \\ & & & \ddots & \ddots & \ddots & & \\ & & & & -\frac{1}{2} & 1 & -\frac{1}{2} & \\ & & & & & -\frac{1}{2} & 1 \end{bmatrix} \begin{bmatrix} r_{1,j} \\ r_{2,j} \\ \vdots \\ r_{j-1,j} \\ r_{j,j} \\ r_{j+1,j} \\ \vdots \\ r_{N+1,j} \end{bmatrix} = \begin{bmatrix} 0 \\ 0 \\ \vdots \\ 0 \\ 1 \\ 0 \\ \vdots \\ 0 \end{bmatrix}.$$

In the basis step we will show that this holds for $i=1$. In the inductive step we will show that this holds for $i>j$, $i<j$ and $i=j$.

Basis step: When $i=1$, the first equation is $r_{1,j}-\frac{1}{2}r_{2,j}=0$ for which we have $r_{2,j}=2r_{1,j}$ and Eq. (20) holds.

Induction step: We assume that Eq. (20) hold for all j on the interval $i>j\geq k-1>1$. We have $-\frac{1}{2}r_{k-1,j}+r_{k,j}-\frac{1}{2}r_{k+1,j}=0$ and if we fill in elements from Eq. (20) we see that the equation holds for $i\geq j$. Similarly we can show then when $i<j$ the equation also holds. The last thing left is to determine $r_{j,j}$. From the jth equation we have $-\frac{1}{2}r_{j-1,j}+r_{j,j}-\frac{1}{2}r_{j+1,j}=1$. With $r_{j-1,j}=\frac{2(j-1)(N+1-j)}{N+1}$, $r_{j,j}=\frac{2j(N+1-j)}{N+1}$ and $r_{j+1,j}=\frac{2j(N+1-(j+1))}{N+1}$, we can show that the equation holds. □

References

[1] P.J. Buist, P.J.G. Teunissen, P. Joosten, GNSS-guided relative positioning and attitude determination for missions with multiple spacecraft, in: Proceedings of GPS/GNSS Symposium, Tokyo, Japan, 15–17 November 2006.

[2] I. Kawano, M. Mokuno, T. Kasai, T. Suzuku, First autonomous rendezvous using relative GPS navigation by ETS-VII, in: ION-GPS Conference, Nashville, TN, US, 14–17 September 1999.

[3] E. Gill, O. Montenbruck, S. DAmico, S. Persson, Autonomous satellite formation flying for the PRISMA technology demonstration mission, in: 16th AAS/AIAA Space Flight Mechanics Conference, Tampa, Florida, 22–26 January 2006.

[4] R. Kroes, Precise relative positioning of formation flying spacecraft using GPS, Ph.D. Thesis, Delft, The Netherlands, March 2006.

[5] P.J. Buist, S. Kumagai, T. Ito, K. Hama, K. Mitani, Development of the integrated navigation unit; combining a GPS receiver with star sensor measurements, in: Proceedings of the 10th International Conference of Pacific Basin Societies (ISCOPS), vol. 117, 2003.

[6] Y. Ishijima, T. Miyano, T. Ito, P.J. Buist, GPS attitude determination field test and preliminary analysis results using on-orbit GPS data of ETS-VII, in: International Workshop on Aerospace Applications of the Global Positioning System, Breckenridge, Co, US, 31 January–2 February 2000.

[7] Narmada, ATV-Far rendez-vous navigation based on relative GPS, in: Proceedings of ION GPS-2005, Long Beach, CA, US, 13–16 September 2005.

[8] H. Marcille, G. Moreau, V. Pascal, Relative GPS navigation design and validation for ATV rendez-vous, in: Proceedings of the 3rd ESA International Conference on Spacecraft Guidance, Navigation and Control Systems, ESA SP-381, November 26–29, ESTEC, Noordwijk, The Netherlands, 1997, p. 77.

[9] P. Saunders, G. Barton, GPS on the International Space Station Alpha, in: Proceedings of the 1995 National Technical Meeting of ION, 18–20 January 1995, Anaheim, CA, US, 1995.

[10] Surrey supplies GPS unit for International Space Station, ⟨http://www.spaceref.com/news/viewpr.html?pid=6243⟩, 2009.

[11] D. Svehla, M. Rothacher, C. Salomon, G. Beyerle, J. Wickert, M. Ziebart, J. Dow, L. Cacciapuoti, T. Boerner, A. Rius, F. Cardellach, O. Montenbruck, R. Rivas, T. Gruber, C. Shum, P. Hoeg, T. Neubert, A. Helm, J. Hahn, I. Prochazka, U. Schreiber, P. Lauber, U. Hugentobler, W. Schäfer, Galileo onboard the International Space Station, in: 2nd International Colloquium on Scientific and Fundamental Aspects of the Galileo Program, Padua, Italy, 14–16 October 2009.

[12] S. Gomez, M. Lammers, Lessons learned from two years of on-orbit global positioning system experience on International Space Station, in: Proceedings of the Institute of Navigation Global Navigation Satellite Systems Conference (GNSS 2004), Long Beach, CA, US, 21–24 September 2004.

[13] J. Tsukui, S. Hotta, T. Imada, K. Yamanaka, T. Kasai, Automatic rendezvous to the International Space Station, in: Proceeding of the 7th International Symposium on Artificial Intelligence, Robotics and Automation in Space: i-SAIRAS 2003, NARA, Japan, 19–23 May 2003.

[14] O. Montenbruck, P.W.L. van Barneveld, Y. Yoon, P.N.A.M. Visser, GPS-based precision baseline reconstruction for the TanDEM-X SAR-Formation, in: 20th International Symposium on Space Flight Dynamics, September 24–28, Annapolis, US, 2007.

[15] S. Mitani, T. Yamamoto, I. Kawano, S. Sakai, H. Tsunemi, FFAST team, FFAST: formation flight all sky telescope, Formation Flight System Analyses and Design, 27th ISTS (International Symposium on Space Technology and Science), Tsukuba, Japan, 5–12 July 2009.

[16] J.-S. Ardaens, O. Montenbruck, S. DAmico, Functional and performance validation of the prisma precise orbit determination facility, in: Proceedings of ION 2010 International Technical Meeting, San Diego, CA, US, 25–27 January 2010.

[17] P.J.G. Teunissen, A. Kleusberg, GPS for Geodesy, Springer, Berlin, Heidelberg, New York, 1998.

[18] P.J.G. Teunissen, The least-squares ambiguity decorrelation adjustment: a method for fast GPS integer ambiguity estimation, Journal of Geodesy 70 (1995) 65–82.

[19] P.J.G. Teunissen, The success rate and precision of GPS ambiguities, Journal of Geodesy 74 (2000) 321–326.

[20] P.J.G. Teunissen, The parameter distributions of the integer GPS model, Journal of Geodesy 76 (2002) 41–48.

[21] S. Verhagen, P.J.G. Teunissen, New global navigation satellite system ambiguity resolution method compared to existing approaches, Journal of Guidance, Control, and Dynamics 29 (2006) 981–991.

[22] P.J.G. Teunissen, The LAMBDA method for the GNSS compass, Artificial Satellites 41 (2006) 89–103.

[23] P.J. Buist, The baseline constrained LAMBDA method for single epoch, single frequency attitude determination applications, in: Proceedings of ION GPS-2007, 2007, pp. 2962–2973.

[24] P.J.G. Teunissen, Integer least squares theory for the GNSS compass, Journal of Geodesy, 84 (7) 433–447, doi:10.1007/s00190-010-0380-8.

[25] P.J.G. Teunissen, G. Giorgi, P.J. Buist, Testing of a new single-frequency GNSS carrier-phase attitude determination method: land, ship and aircraft experiments, GPS Solutions, doi:10.1007/s10291-010-0164-x, 2010.

[26] C. Park, P.J.G. Teunissen, A new carrier phase ambiguity estimation for GNSS attitude determination systems, in: Proceedings of International GPS/GNSS Symposium, Tokyo, 15–18 November 2003.

[27] P.J. Buist, GNSS kinematic relative positioning for spacecraft: data analysis of a dynamic testbed, in: 26th ISTS (International Symposium on Space Technology and Science), Hamamatsu, Japan, 1–8 June 2008.

[28] P.J. Buist, P.J.G. Teunissen, G. Giorgi, S. Verhagen, Instantaneous multi-baseline ambiguity resolution with constraints, in: International Symposium on GPS/GNSS 2008, Tokyo, Japan, 11–14 November 2008.

[29] P.J. Buist, P.J.G. Teunissen, G. Giorgi, S. Verhagen, Multiplatform instantaneous GNSS ambiguity resolution for triple- and quadruple-antenna configurations with constraints, International Journal of Navigation and Observation, vol. 2009, Article ID 565426, 14pp, doi:10.1155/2009/565426, 2009.
[30] P.J.G. Teunissen, A general multivariate formulation of the multi-antenna GNSS attitude determination problem, Artificial Satellites 42 (2007) 97–111.
[31] G. Giorgi, P.J.G. Teunissen, Carrier phase GNSS attitude determination with the multivariate constrained LAMBDA method, in: Proceedings of IEEE-AIAA Aerospace Conference, Big Sky, MT, US, 2010 p. 12.
[32] G. Giorgi, P.J.G. Teunissen, S. Verhagen, P.J. Buist, Testing a new multivariate GNSS carrier phase attitude determination method for remote sensing platforms, Advances in Space Research 46 (2) (2010) 118–129, doi:10.1016/j.asr.2010.02.023.
[33] S. Verhagen, Visualization of GNSS-related design parameters: Manual for the Matlab user interface VISUAL, 2006.
[34] J. Leyssens, M. Markgraf, Evaluation of a commercial-off-the-shelf dualfrequency GPS receiver for use on LEO satellites, in: Proceedings of the 18th International Technical meeting of the Institute of Navigation Satellite Division, ION-GNSS-2005, Long Beach, CA, US, 13–16 September 2005.
[35] M. Manzano-Jurado, C. Carrascosa-Sanz, A. Garcia-Rodrígues, Formation flying LEO test bed at the ESTEC navigation laboratory, in: 4th ESA Workshop on Satellite Navigation User Equipment Technologies, NAVITEC, Noordwijk, The Netherlands, 10–12 December 2008.
[36] R.L. Burden, J.D. Faires, A.C. Reynolds, Numerical Analysis, Prindle, Weber and Schmidt, Boston, 1978.
[37] T. Maruyama, Stochastic Problems in Population Genetics, Springer, 1977.
[38] G. Meurant, A review on the inverse of symmetric tridiagonal and block tridiagonal matrices, SIAM Journal on Matrix Analysis and Applications 13 (1992) 707.